Research on Engineering Structures & Materials
www.jresm.org
Research Group

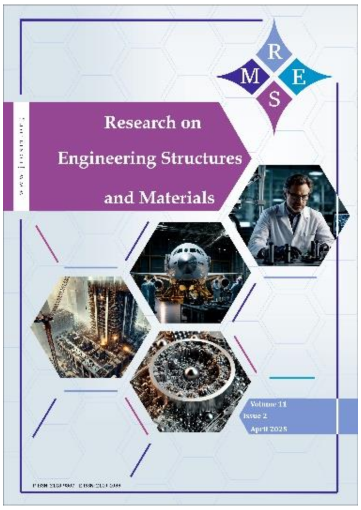


# A multi-response optimization of ternary geopolymer mortar using Taguchi–GRA integrated method

Surya Teja Chinnala, Sai Kumar Vindula

Online Publication Date: 20 February 2026

URL: http://www.jresm.org/archive/resm2026-1441ma1227rs.html
DOI: http://dx.doi.org/10.17515/resm2026-1441ma1227rs

Journal Abbreviation: *Res. Eng. Struct. Mater.*

**To cite this article**
Chinnala S T, Vindula S K. A multi-response optimization of ternary geopolymer mortar using Taguchi–GRA integrated method. *Res. Eng. Struct. Mater.*, 2026; 12(4): 2417-2433.

Research on Engineering Structures & Materials
www.jresm.org
Research Group

*Research Article*

# A multi-response optimization of ternary geopolymer mortar using Taguchi–GRA integrated method

Surya Teja Chinnala [a], Sai Kumar Vindula *,[b]

*Department of Civil Engineering, GITAM School of Core Engineering, GITAM Deemed to be University, Visakhapatnam - 530045, India*

**Article Info**

***Article History:***

Received 27 Dec 2025

Accepted 17 Feb 2026

***Keywords:***

Red mud;
Geopolymer mortar;
Compressive strength;
Taguchi-GRA integrated method

**Abstract**

This research addresses a critical gap in sustainable binder development by integrating experimental optimization and multi-response analysis to assess the performance of ternary Red Mud–Ground Granulated Blast Furnace Slag–Metakaolin (RM–GGBS–MK) geopolymer mortars. Although geopolymers are recognized for their potential to reduce cement consumption and $CO_2$ emissions, limited studies have systematically optimized ternary waste-based binders considering both fresh and hardened properties. In this study, a hybrid Taguchi–Grey Relational Analysis (GRA) framework was employed to simultaneously optimize the compressive strength, flowability, and setting times of geopolymer mortar mixes under three criteria: balanced performance, strength, and workability. The experimental design followed an L16 orthogonal array comprising five parameters—ternary composition, NaOH molarity, activator-to-binder (AL/B) ratio, $Na_2SiO_3$/NaOH (SS/SH) ratio, and binder-to-sand (B/S) ratio—each at four levels. The GGBS-rich mixes attained the maximum compressive strength of 49.09 MPa at 28 days, whereas the RM and MK dominant mixes demonstrated diminished strengths comparatively. ANOVA results indicated the most significant factors affecting the strength and flowability as SS/SH and Al/B ratios, whereas the binder compositions regulated initial and final setting times. Across all three criteria, GRA identified 14 M NaOH and a 1:1.5 B/S ratio as common significant parameters.



## 1. Introduction

Cement production contributes to around 8% of worldwide $CO_2$ emissions[1]. This global challenge has prompted research into alternative binders that can diminish the carbon footprint of cement production. By utilizing industrial wastes, geopolymers have emerged as sustainable replacements[2]. Aluminosilicate-rich industrial by-products are activated with alkaline solutions to form geopolymers[3].Compared with ordinary Portland cement (OPC), these materials exhibit enhanced physical and mechanical performance.

Red Mud (RM), an alkaline by-product of the Bayer process used in alumina production, is generated in substantial amounts globally and poses significant environmental disposal challenges [4]. In India, the annual generation of red mud is approximately 9 to 12 million metric tons [5]. RM contains high levels of $Fe_2O_3$ and $Al_2O_3$, while showing a lower concentration of reactive $SiO_2$, thereby limiting its geopolymer reactivity. [6] When used alone as a binder, RM often requires thermal curing and shows minimal early strength development. RM stored in landfills may pose environmental risks due to high alkalinity, which can lead to soil and water contamination [7].

*Corresponding author: svindula@gitam.edu
[a]orcid.org/0000-0001-5597-4740; [b]orcid.org/0000-0002-1301-4378
DOI: http://dx.doi.org/10.17515/resm2026-1441ma1227rs

Ground Granulated Blast Furnace Slag (GGBS) is an industrial by-product produced from blast furnaces utilized in iron manufacturing. This material is abundant in aluminosilicates and CaO, rendering it an appropriate source for geopolymer binders. It improves geopolymer characteristics by accelerating strength attainment and diminishing the necessity for thermal curing [8,9]. The annual production of GGBS in India is estimated at approximately 15 million tons[10]. Although majority of GGBS is used as supplementary cementitious material, unused GGBS creates significant pollution in the form of airborne particulate matter.

Proportions of oxides such as $SiO_2$, $Al_2O_3$, $Fe_2O_3$ and CaO strongly influence the performance of geopolymer binders [11]. Industrial by-products like RM and GGBS vary in chemical compositions, and their combined use may not always provide sufficient reactive silica and alumina for optimal geopolymerization. Metakaolin (MK), a highly reactive aluminosilicate obtained by calcining kaolinite clay at elevated temperatures, is incorporated to supplement these oxides. By enhancing reactive Si and Al, MK promotes the development of stronger and more durable geopolymer matrix[12,13].

Geopolymer mortar properties are affected by multiple factors such as molarity of the NaOH, alkaline activator to binder (Al/B) ratio, binder to aggregate proportions, and curing conditions [14]. Binary mixes comprising RM-GGBS and RM-MK have been studied previously in the literature. RM–GGBS blends benefit from calcium-induced strength gain and reduced curing temperature but can suffer from quick setting times and workability when RM content is high[15]. RM–MK blends improve the Si and Al content but lack calcium for rapid early strength [16]. Wang et.al[17] had demonstrated that mixtures containing 60–70% GGBS, with Red Mud as a secondary component, attained compressive strengths greater than 45 MPa, with enhanced thermal resistance and matrix densification. The use of Metakaolin at 60%, in conjunction with RM, has demonstrated a significant improvement in long-term strength and microstructural integrity[18,19]. In addition to these findings, RM-rich blends consisting of 60% Red Mud and 40% GGBS exhibited compressive strengths between 30 and 38 MPa [20,21]. Nevertheless, few studies have been done on the combined impact of all the three binders. The ternary mix presents a promising option for a sustainable substitute for cement [22].

The Taguchi approach along with Grey Relational Analysis (GRA), has been utilized to efficiently study and optimize multiple parameters in geopolymer systems, including strength, setting time, and workability [23,24]. Orthogonal arrays (OA) are employed in Taguchi method to identify critical factors and minimize the number of experimental trials[25–27]. The GRA enhances the Taguchi approach by facilitating multi-response optimization, aiding in the identification of parameter combinations that balance fresh state and hardened state properties [28]. The GRA consolidates various performance attributes into a singular Grey Relational Grade, hence easing the optimization procedure[29,30]. It facilitates the identification of optimal factor levels by ranking the Grey Relational Grades, consequently revealing the parameter configurations that yield superior overall performance.

This study investigates the influence of mix parameters on the performance characteristics of RM–GGBS–MK geopolymer mortar. The factors considered include the sodium silicate to sodium hydroxide (SS/SH) ratio, NaOH molarity, Al/B ratio, and binder to sand ratio, with the ternary mix composition (different proportions of binders) included as one of the factors due to its influence on aluminosilicate availability and geopolymerization. Taguchi design of experiments combined with GRA was employed to determine optimal parameter combinations under ambient curing conditions for multi-response optimization under three different optimization objectives corresponding to strength, workability, and balanced overall performance.

## 2. Materials

RM was obtained from NALCO, Damanjodi, Odisha. RM is predominantly composed of $Fe_2O_3$ and $Al_2O_3$ and has a characteristic red color. It was oven-dried at 80$^o$C for a minimum of 24 hours to remove moisture, and the dried lumps were grounded and sieved through a 75-micron sieve. GGBS was sourced from Visakhapatnam. It is rich in calcium silicates and acts as a significant source of CaO, and has a greyish-white color. MK was sourced from Mumbai, India. It is a highly reactive aluminosilicate material with good pozzolanic properties. It has an off-white colour. The chemical compositions of RM, GGBS and MK as determined by X-ray fluorescence (XRF) analysis are presented in Table 1, while their particle size distribution and XRD details are presented in Figure 1. XRD pattern of MK exhibits a large diffuse hump alongside identifiable crystalline peaks primarily attributed to quartz (Q). RM sample displays distinct diffraction peaks corresponding to gibbsite (G) and hematite (H) as the primary crystalline phases, alongside modest reflections of quartz (Q) and weak carbonate (C). The XRD pattern of GGBS is characterized by a large amorphous halo, usually found in the 2θ range of about 20–35°, indicating the prevalence of glassy amorphous phases in the slag.

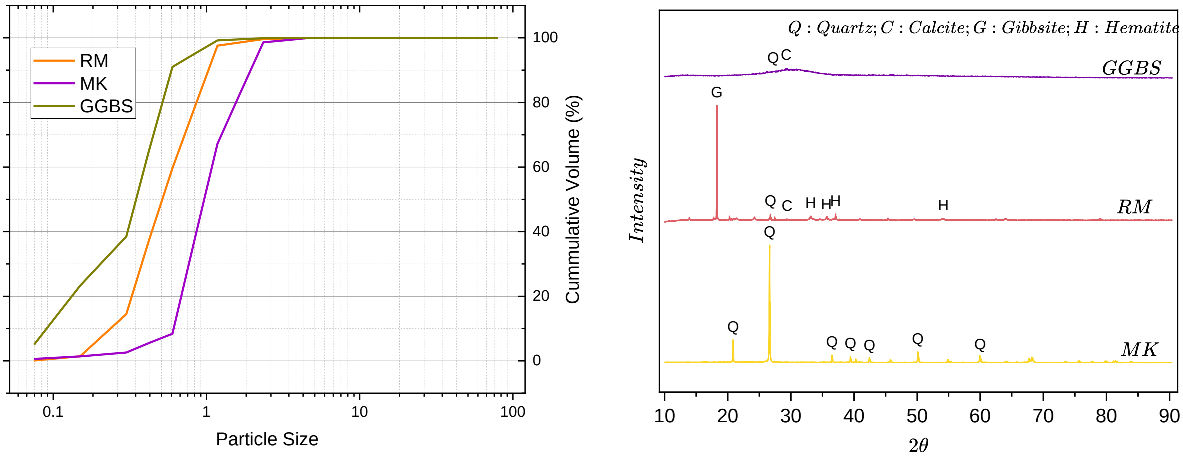


Fig. 1. Particle size distribution and XRD of the binder materials

Commercially available sodium silicate and sodium hydroxide solutions were used as alkaline activators in this study. SS/SH ratio was considered as a variable affecting the geopolymer mortar properties. Sodium hydroxide (NaOH) pellets with 99% purity were dissolved in water for 24 hours, prior to casting. Sodium silicate solution comprised of 26.5 wt% $SiO_2$ and 8.0 wt% $Na_2O$. River sand conforming to Grade 2 as per IS:383 [31] was used as fine aggregate. Binder-to-sand ratio was considered as one of the experimental factors, due to its influence on the strength of mortar.

Table 1. Chemical compositions of binder materials

| Materials | $Al_2O_3$ | CaO | $SiO_2$ | MgO | $Na_2O$ | $K_2O$ | $Fe_2O_3$ | $TiO_2$ |
|---|---|---|---|---|---|---|---|---|
| RM | 15.03 | 1.5 | 7.85 | 2.14 | 4.65 | 2.59 | 49.18 | 4.5 |
| GGBS | 10.39 | 38.12 | 32.41 | 8.96 | 0.35 | 0.5 | 0.69 | 1.23 |
| MK | 41.41 | 0.08 | 52.22 | 0.26 | 0.01 | 1.73 | 0.49 | 0.65 |

## 3. Methodology

The methodology employed for single response optimization utilizing Taguchi and multi-response optimization employing GRA is illustrated in Figure 2. In this study, five key factors influencing geopolymerization were selected based on prior literature and preliminary trials. The factors considered include the ternary mix proportions of RM, GGBS, and MK at specified ratios; NaOH at 8, 10, 12 and 14 molarity, Al/B ratio between 0.45 and 0.60, SS/SH ratio from 1.0 to 2.5 and B/S ratio from 1:1.5 to 1:3. Each parameter was chosen based on its impact on the geopolymerization process. The ternary blend ratio and B/S ratio regulates the proportions of reactive alumina, silica and calcium, whereas the molarity of NaOH influences precursor dissolution through the provision of $OH^-$ and $Na^+$ ions[32–34]. The Al/B ratio ensures an adequate amount of activator in relation to the binder, while the SS/SH ratio controls the availability of soluble silica for polycondensation [22,32].

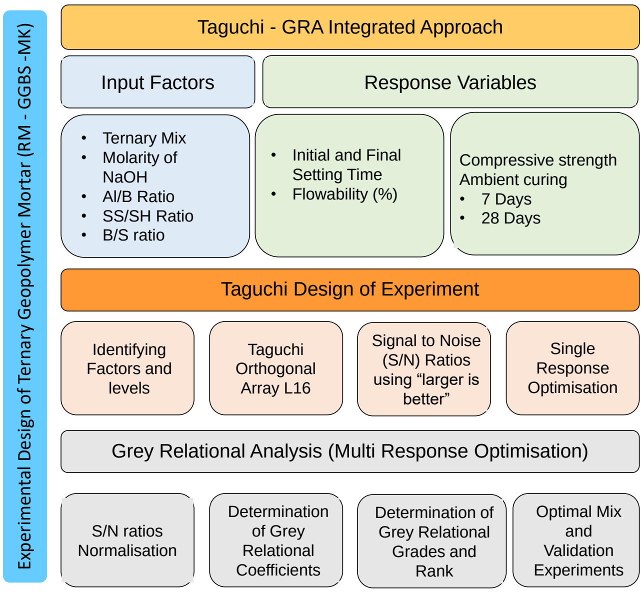


Fig. 2. Flowchart for optimisation methodology

The integrated Taguchi-GRA method is utilized to optimize various performance parameters of ternary RM–GGBS–MK geopolymer mortar. An L16 Taguchi OA is employed to investigate the main factor effects on geopolymer mortar properties. The full factorial design requires 1024 experimental combinations ($4^5$), making the process expensive and time-consuming. The Taguchi method enables systematic evaluation of multiple variables with a reduced number of trials through orthogonal arrays, whereas GRA facilitates multi-response optimization by consolidating different performance attributes into a single comparative index. Factors considered and the corresponding four levels are shown in Table 2. The factor assignments are presented in Table 3.

Table 2. Factors and levels for Taguchi method

| Parameters | Level 1 | Level 2 | Level 3 | Level 4 |
|---|---|---|---|---|
| Ternary Mix | A1-20G60M20 | A2-20G20M60 | A3-60G20M20 | A4-33G33M33 |
| NaOH Molarity | 8 | 10 | 12 | 14 |
| AL/B Ratio | 0.6 | 0.55 | 0.5 | 0.45 |
| SS/SH Ratio | 2.5 | 2 | 1.5 | 1.0 |
| B/S Ratio | 1:3 | 1:2.5 | 1:2 | 1:1.5 |

The Taguchi method evaluates robustness through signal-to-noise (S/N) ratios, which can be determined on the basis of "larger-the-better," "smaller-the-better," or "nominal-the-best" [36]. Since extended setting time, increased compressive strength and higher workability are targeted, the larger-the-better formulation was used for all responses as shown

$$y_{pq} = -10 \times log_{10}\left[\frac{1}{n}\sum\frac{1}{v_{pi}^2}\right] \quad (1)$$

where, $v_{pi}$ is the response of $p^{th}$ trial mix for the $i^{th}$ response and n is the number of observations, $y_{pq}$ denotes the experiment's signal/noise ratio.

ANOVA was performed on S/N ratios to enumerate the effect of each factor. As the OA, had zero degrees of freedom. Hence, factor contributions were considered as the percentage of the sum of squares [37].

Table 3. Mix compositions and factor levels

| Mix | Ternary Mix | NaOH Molarity | AL/B Ratio | SS/SH Ratio | B/S Ratio |
|---|---|---|---|---|---|
| M1 | R20G60M20 | 8 | 0.6 | 2.5 | 1:3 |
| M2 | R20G60M20 | 10 | 0.55 | 2 | 1:2.5 |
| M3 | R20G60M20 | 12 | 0.5 | 1.5 | 1:2 |
| M4 | R20G60M20 | 14 | 0.45 | 1 | 1:1.5 |
| M5 | R20G20M60 | 8 | 0.55 | 1.5 | 1:1.5 |
| M6 | R20G20M60 | 10 | 0.6 | 1 | 1:2 |
| M7 | R20G20M60 | 12 | 0.45 | 2.5 | 1:2.5 |
| M8 | R20G20M60 | 14 | 0.5 | 2 | 1:3 |
| M9 | R60G20M20 | 8 | 0.5 | 1 | 1:2.5 |
| M10 | R60G20M20 | 10 | 0.45 | 1.5 | 1:3 |
| M11 | R60G20M20 | 12 | 0.6 | 2 | 1:1.5 |
| M12 | R60G20M20 | 14 | 0.55 | 2.5 | 1:2 |
| M13 | R33G33M33 | 8 | 0.45 | 2 | 1:2 |
| M14 | R33G33M33 | 10 | 0.5 | 2.5 | 1:1.5 |
| M15 | R33G33M33 | 12 | 0.55 | 1 | 1:3 |
| M16 | R33G33M33 | 14 | 0.6 | 1.5 | 1:2.5 |

The following equation was used to normalize the signal-to-noise ratio for each result;

$$Z_{pq} = \frac{y_{pq} - min(y_{pq})}{max(y_{pq}) - min(y_{pq})}; p = 1,2,\dots,r; q = 1,2,\dots,n \tag{2}$$

Grey Relational Coefficient (GRC) was calculated using the following equation;

$$GRC_{0pq} = \frac{\Delta_{min} + \varsigma\Delta_{max}}{\Delta_{0pq} + \varsigma\Delta_{max}} \tag{3}$$

$\Delta_{0pq}$ represents the discrepancy between the ideal and actual values of the normalized signal-to-noise ratio. The variable ς denotes the identification or distinguishing coefficient, which ranges from 0 to 1, typically set at 0.5. [32]. Grey Relational Grade (GRG) was determined using;

$$GRG_{opq} = \frac{1}{n}\sum_{n=1}^{m} wGRC_{opq}; p = 1,2,\dots,r \tag{4}$$

For various multi-response optimization objectives, suitable weighting factors were allocated to the response variables, and the Grey Relational Grade (GRG) was computed by the weighted aggregation of the respective Grey Relational Coefficients (GRCs).

### 3.1 Mix Procedure

The RM, GGBS, and MK were dry-mixed with fine aggregate for two minutes in a mortar mixer. The pre-prepared SS+SH alkaline solution was subsequently added, and the process was carried out for three minutes. The mortar was poured into 70.6 mm cube moulds as shown in Figure 3, compacted, and subjected to vibration for a duration of two minutes. 03 specimens for each mix were demoulded and stored at room temperature until testing at 7 and 28 days at an average temperature of 29$^{o}$C. Flowability (%) for the mortar samples was determined according to IS 5512[39]. Tests for setting times were conducted as per IS 4031-Part 5[40]. Tests for compressive strength were carried out according to IS: 516[41]. The Bruker D8 Advance diffractometer is employed for X-ray diffraction investigation to examine crystalline structure and phase composition. Phase identification was achieved by correlating diffraction patterns with standard reference cards. The Bruker ALPHA-II ATR-FTIR spectrophotometer is employed for FTIR analysis.

Fig. 3. Geopolymer mortar specimens

## 4. Results and Discussion

S/N ratios and the experimental results for setting time, flowability, and compressive strength for all mixes are displayed in Table 4a and 4b. The results were evaluated by computing the average S/N ratio for each individual response across all the mixes with identical factors.

Table 4. (a) S/N ratios of the response variables

| Mix Designation | Ternary Mix | NaOH Molarity | Al/B | SS/SH | B/S | S/N Ratios | | | | |
|---|---|---|---|---|---|---|---|---|---|---|
| | | | | | | Flow | IST | FST | CS-07 Days | CS -28 Days |
| M1 | A1 | 8 | 0.6 | 2.5 | 1:3 | 41.41 | 32.67 | 35.99 | 27.74 | 31.37 |
| M2 | A1 | 10 | 0.55 | 2 | 1:2.5 | 38.59 | 34.96 | 40.91 | 27.02 | 21.42 |
| M3 | A1 | 12 | 0.5 | 1.5 | 1:2 | 34.81 | 38.59 | 46.24 | 20.87 | 28.63 |
| M4 | A1 | 14 | 0.45 | 1 | 1:1.5 | 43.52 | 34.32 | 39.09 | 33.25 | 33.82 |
| M5 | A2 | 8 | 0.55 | 1.5 | 1:1.5 | 43.52 | 47.24 | 50.93 | 24.35 | 28.80 |
| M6 | A2 | 10 | 0.6 | 1 | 1:2 | 39.65 | 45.80 | 48.13 | 23.33 | 27.95 |
| M7 | A2 | 12 | 0.45 | 2.5 | 1:2.5 | 43.52 | 36.26 | 41.94 | 28.28 | 30.29 |
| M8 | A2 | 14 | 0.5 | 2 | 1:3 | 27.96 | 50.32 | 52.42 | 15.04 | 18.57 |
| M9 | A3 | 8 | 0.5 | 1 | 1:2.5 | 33.06 | 45.58 | 49.13 | 22.15 | 24.88 |
| M10 | A3 | 10 | 0.45 | 1.5 | 1:3 | 31.36 | 45.58 | 45.34 | 16.22 | 26.82 |
| M11 | A3 | 12 | 0.6 | 2 | 1:1.5 | 41.18 | 52.67 | 55.71 | 16.83 | 22.29 |
| M12 | A3 | 14 | 0.55 | 2.5 | 1:2 | 43.52 | 46.44 | 50.26 | 23.89 | 21.18 |
| M13 | A4 | 8 | 0.45 | 2 | 1:2 | 34.85 | 33.98 | 40.91 | 30.23 | 29.07 |
| M14 | A4 | 10 | 0.5 | 2.5 | 1:1.5 | 43.52 | 40.83 | 43.81 | 24.06 | 28.74 |
| M15 | A4 | 12 | 0.55 | 1 | 1:3 | 43.52 | 39.55 | 47.78 | 26.22 | 27.18 |
| M16 | A4 | 14 | 0.6 | 1.5 | 1:2.5 | 43.52 | 38.79 | 45.85 | 17.01 | 28.82 |

Table 4. (b) Experimental results of response variables

| Mix Designation | Setting Time Initial, mins | Setting Time Final, mins | Flowability (%) | 07 Days Compressive Strength Strength, MPa | 07 Days Std. Deviation | 07 Days Coefficient of Variation | 28 Days Compressive Strength Strength, MPa | 28 Days Std. Deviation | 28 Days Coefficient of Variation |
|---|---|---|---|---|---|---|---|---|---|
| M1 | 43 | 63 | 117.6 | 24.38 | 0.872 | 3.57% | 37.02 | 1.758 | 4.75% |
| M2 | 56 | 111 | 85 | 22.45 | 2.227 | 9.92% | 11.78 | 1.054 | 8.94% |
| M3 | 85 | 205 | 55 | 11.05 | 1.039 | 9.41% | 27.02 | 1.453 | 5.38% |
| M4 | 52 | 90 | 150 | 45.96 | 2.242 | 4.88% | 49.09 | 6.145 | 12.52% |
| M5 | 230 | 352 | 150 | 16.5 | 0.919 | 5.57% | 27.54 | 2.539 | 9.22% |
| M6 | 195 | 255 | 96 | 14.67 | 0.544 | 3.71% | 24.98 | 1.932 | 7.73% |
| M7 | 65 | 125 | 150 | 25.94 | 0.983 | 3.79% | 32.71 | 3.903 | 11.93% |
| M8 | 328 | 418 | 25 | 5.65 | 0.344 | 6.09% | 8.48 | 0.397 | 4.68% |
| M9 | 190 | 286 | 45 | 12.81 | 0.911 | 7.11% | 17.53 | 1.236 | 7.05% |
| M10 | 190 | 185 | 37 | 6.47 | 0.13 | 2.01% | 21.93 | 0.453 | 2.06% |
| M11 | 430 | 610 | 114.5 | 6.94 | 0.622 | 8.96% | 13.02 | 1.073 | 8.24% |
| M12 | 210 | 326 | 150 | 15.65 | 0.283 | 1.81% | 11.45 | 0.898 | 7.84% |
| M13 | 50 | 111 | 55.25 | 32.48 | 1.62 | 4.99% | 28.4 | 1.803 | 6.35% |
| M14 | 110 | 155 | 150 | 15.95 | 0.64 | 4.01% | 27.36 | 0.979 | 3.58% |
| M15 | 95 | 245 | 150 | 20.46 | 0.276 | 1.35% | 22.86 | 3.055 | 13.36% |
| M16 | 87 | 196 | 150 | 7.09 | 0.212 | 2.99% | 27.59 | 2.807 | 10.17% |

## 4.2 Compressive Strength

The compressive strength test was carried out for each of the 16 mixes designed through the Taguchi method. Figure 4 shows the computed average compressive strength. At all the curing intervals, Mix M4 (60% GGBS and 20% RM & MK, Molarity: 14, Al/B ratio: 0.45, SS/SH ratio: 1, and B/S ratio: 1:1.5) demonstrated the highest compressive strength. Mix M8 (60% RM, 20% GGBS & MK, Molarity: 14, Al/B ratio: 0.55, SS/SH ratio: 2, B/S ratio: 1:3) exhibited the lowest compressive strength.

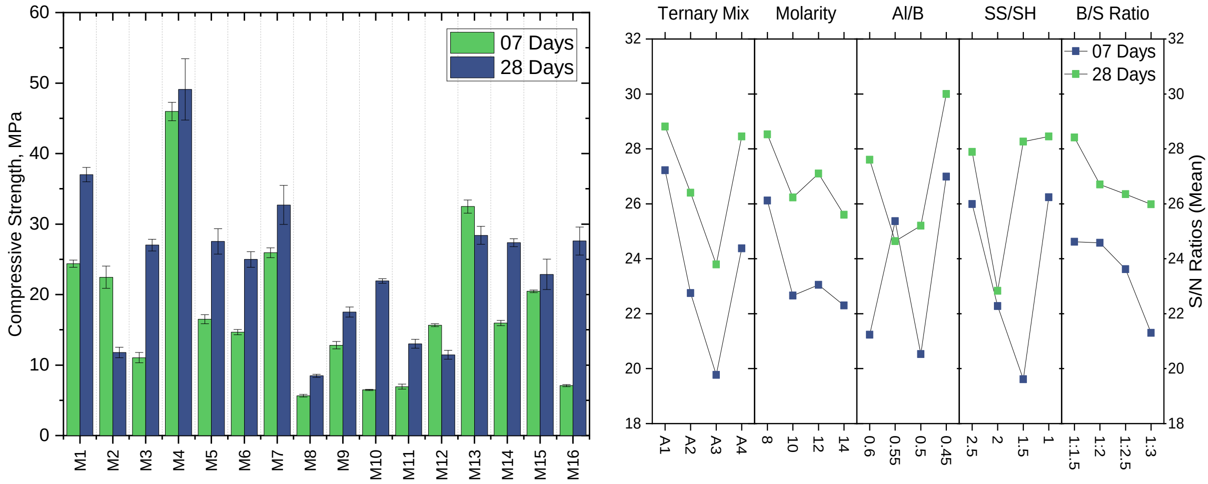


Fig. 4. Compressive strength and S/N ratios (mean)

From Figure 4, the ternary mixes with 60% GGBS had a pronounced effect on the compressive strength. Mixes comprising 60% RM and 60% MK had notable reduction in strength. As evident from Table 4, increasing the GGBS content from 20% to 60% resulted in improved compressive strength. The total calcium content of the mixes increased with increase in GGBS content. Thus, improving the solubility of raw materials which facilitates enhanced geopolymerization producing supplementary C-A-S-H, N-A-S-H and C-S-H gels [42–44].

From the previous literature, the relationship between molarity and strength is uncertain. Certain studies indicate that higher molarity of NaOH correlates with increased compressive strength whereas other studies has shown that elevated NaOH concentration may result in decreased compressive strength [45,46]. Source of aluminosilicate is a critical factor in determining the optimal NaOH concentration [47]. 8 Molar alkaline activators have exhibited higher compressive strength. In this study, increasing molarity resulted in decreased compressive strength, with the exception of 12 molar NaOH. Total amount of alkaline solution in the system is directly proportional to Al/B ratio. The maximum compressive strength was determined for Al/B ratio of 0.45. Increase in Al/B ratio results an inconsistent pattern in compressive strength. Excess alkaline activator contributed to an increased water content in the mixture, which inhibited geopolymerization[48]

Figure 4 shows the S/N ratio (mean) for various SS/SH ratios, the result doesn't follow a consistent pattern. Certain literature indicates that increased silicates due to increased SS/SH ratio leads to an increased strength whereas others indicate the opposite, reduction in strength [49,50]. In the present study, SS/SH ratio of 1 exhibited superior performance. From the mean S/N ratios for binder to sand ratio of 1: 1.5 has resulted in enhanced compressive strength. Increase in B/S ratio generally leads to decrease in the compressive strength which might be due to insufficient aluminosilicate [51] as its associated with a decrease in binder content and an increase in fine aggregate content.

Table 5 presents the results of the ANOVA for the compressive strength. The SS/SH, Al/B ratio, and binder materials together contributed to 84.41% and 87.07% of the strength at 7 and 28 days, respectively. The optimization of individual factors for compressive strength involves a geopolymer mortar mix which comprises 60% GGBS, 20% MK and RM, with 8 Molar NaOH, an Al/B ratio of 0.45, an SS/SH ratio of 1.5, and a B/S ratio of 1:1.5.

Table 5. ANOVA analysis for compressive strength

| | CS-07 Days | | | | CS-28 Days | | | |
|---|---|---|---|---|---|---|---|---|
| Factors | $SS_m$ | $SS_t$ | Mean SS | % Contribution | $SS_m$ | $SS_t$ | Mean SS | % Contribution |
| Ternary Mix | 116.28 | 422.08 | 38.76 | 27.55 | 63.88 | 256.44 | 21.29 | 24.91 |
| Molarity | 36.84 | | 12.28 | 8.73 | 19.32 | | 6.44 | 7.53 |
| Al/B | 118.8 | | 39.6 | 28.15 | 72.24 | | 24.08 | 28.17 |
| SS/SH | 121.16 | | 40.39 | 28.71 | 87.16 | | 29.05 | 33.99 |
| B/S | 29 | | 9.67 | 6.87 | 13.84 | | 4.61 | 5.4 |
| Total | 422.08 | | | 100 | 256.44 | | | 100 |

### 4.3 Setting Time

The initial and final setting times of the 16 mixes are shown in Figure 5. Ternary Mixes (M9-M12) containing 60% RM have higher setting times and ternary mixes (M1-M4) with 60 % GGBS have the least setting times, which is in confirmatory with the literature [51]. Prolonged setting time can be attributed to an increase in the RM Content, which results in extended setting time[52] along with higher Al/B ratio[17]. An increase in the CaO owing to increased GGBS shortens the setting times[53] and higher B/S ratio which reduces the binder quantity.

S/N ratios (mean) for the initial and final setting times decreased with increase in the GGBS content (A3, A2 - A4 - A1) which is in line with previous studies[54,55]. The accessible calcium in GGBS provides heterogeneous nucleation sites, expediting the GPZ and leading to a reduced setting time. Consequently, GGBS engages with the alkaline solution more rapidly [53] [56]. The elevated alkalinity of Bayer's red mud may influence the reaction kinetics, potentially resulting in an extended setting time.[57]. From Figure 4, the setting times increased with increase in NaOH Molarity, except for the final setting time which slightly decreases after 12 Molar, which is in line with the previous studies[38] . An increase in Al/B ratio from 0.45 to 0.5 resulted in enlarged setting times[58]. However, this effect from 0.5 to 0.6 is not significant. Increase in the AL/B ratio results in dilution of the alkaline solution, potentially leading to a slowdown in the geopolymerization and in delay of the setting time [59]. Increase in the SS/SH ratio results in increased setting times upto a threshold ratio of 2, after which a substantial decline is observed at the ratio of 2.5. An increased SS/SH and Al/B ratio enhances the soluble $Na^{+}$ ions, thereby facilitating geopolymerization and lower setting times [60]. Changing the B/S ratio from 1:2.5 to 1:1.5 led to increase in the setting times which can be due to the increased binder quantity.

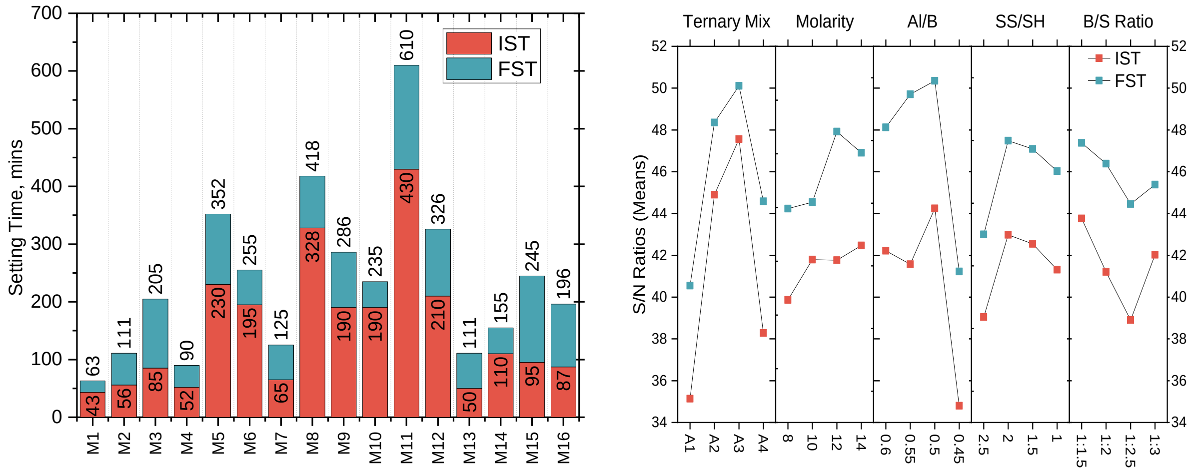


Fig. 5. Setting times of mortars and S/N ratios (means)

Table 6 demonstrates that the Ternary Binder materials is the primary factor influencing the setting times, contributing to 67.49% and 51.85% of the variation in the initial and final setting times, respectively. Al/B ratio is the second most important factor. The optimal mix for setting times is Mix: A3 - 60% RM and 20% GGBS and MK, Molarity: 12, Al/B ratio: 0.45, SS/SH: 2 and B/S ratio: 1:1.5.

Table 6. ANOVA analysis for initial and final setting times

| | Initial Setting Time | | | | Final Setting Time | | | |
|---|---|---|---|---|---|---|---|---|
| Factors | $SS_m$ | $SS_t$ | Mean SS | % Contribution | $SS_m$ | $SS_t$ | Mean SS | % Contribution |
| Ternary Mix | 396.8 | 587.92 | 132.27 | 67.49 | 216.28 | 417.12 | 72.09 | 51.85 |
| Molarity | 15.08 | | 5.03 | 2.56 | 38.68 | | 12.89 | 9.27 |
| Al/B | 89.68 | | 29.89 | 15.25 | 93.56 | | 31.19 | 22.43 |
| SS/SH | 37.32 | | 12.44 | 6.35 | 49.44 | | 16.48 | 11.85 |
| B/S | 49.04 | | 16.35 | 8.34 | 19.16 | | 6.39 | 4.59 |
| Total | 587.92 | | | 100 | 417.12 | | | 100 |

### 4.4 Flowability

Flowability test was used to determine the workability of the geopolymer mortars. For mixes M4, M5, M7, M12, M14- M16 the spread diameter is in excess of the base plate, which is reported as 150%. The least flowability of 25% has been determined for Mix M8. The S/N ratios of flowability as shown in Figure 6 indicate ternary mix with equal proportions of all the binders exhibits the highest flow characteristics, whereas mixes with higher percentages of RM display the least flow. An increase in RM content leads to decreased workability, likely due to the high surface area of RM, which raises water demand [61]. The influence of molarity on the S/N ratio is to enhance the flow up to 12 Molar and then diminish at 14 Molar, although this change is not significant. An increase in NaOH molarity resulted in enhanced flow. An elevated molarity of NaOH results in increase of $OH^{-}$ ions concentration, hence accelerating dissolution and increasing flow[62]. The S/N ratios for flow, plotted alongside the Al/B ratios, indicate a random distribution of performance. The flowability has not decreased with the decrease in the Al/B ratio, which is consistent with previous studies [63,64]. This is due to the complicated action of binders, which effect the flowability [65]. Mixes with Al/B ratio of 0.5 are stiffer compared to mixes with other Al/B ratios. The literature indicates an absence of identifiable trends regarding the influence of the SS/SH ratio. Research indicates that flowability increases as the SS/SH ratio decreases, and conversely, decreases with an increase in the SS/SH ratio[66,67]. The current study indicates that a reduction in SS/SH from 2.5 to 2 results in a significant decrease in flow, while further reductions lead to an increase in flow. The increase in binder quantity led to an increase in flow, with a slight variation observed at a binder-to-sand ratio of 1:2. These variations can be attributed to the enhanced geopolymerization resulting from the increased availability of aluminosilicate materials[68]. Binder content influences inter-particle interactions and solidification, thereby impacting slump values.[38]

Table 7. ANOVA analysis for flowability

| Factors | Flowability | | | |
|---|---|---|---|---|
| | $SS_m$ | $SS_t$ | Mean SS | % Contribution |
| Ternary Mix | 35 | 403.76 | 11.67 | 8.67 |
| Molarity | 17.72 | | 5.91 | 4.39 |
| Al/B | 137.44 | | 45.81 | 34.04 |
| SS/SH | 113.56 | | 37.85 | 28.13 |
| B/S | 100.04 | | 33.35 | 24.78 |
| Total | 403.76 | | | 100 |

From Table 7, it can be concluded that the Al/B, SS/SH, and B/S ratios are the major factors influencing flowability. Al/B ratio is the primary factor influencing 34.04% of the variation. The optimal mix for setting times is Mix: A4 – 33.33% RM, GGBS and MK, Molarity: 12, Al/B ratio: 0.55, SS/SH: 2.5 and B/S ratio: 1:1.5.

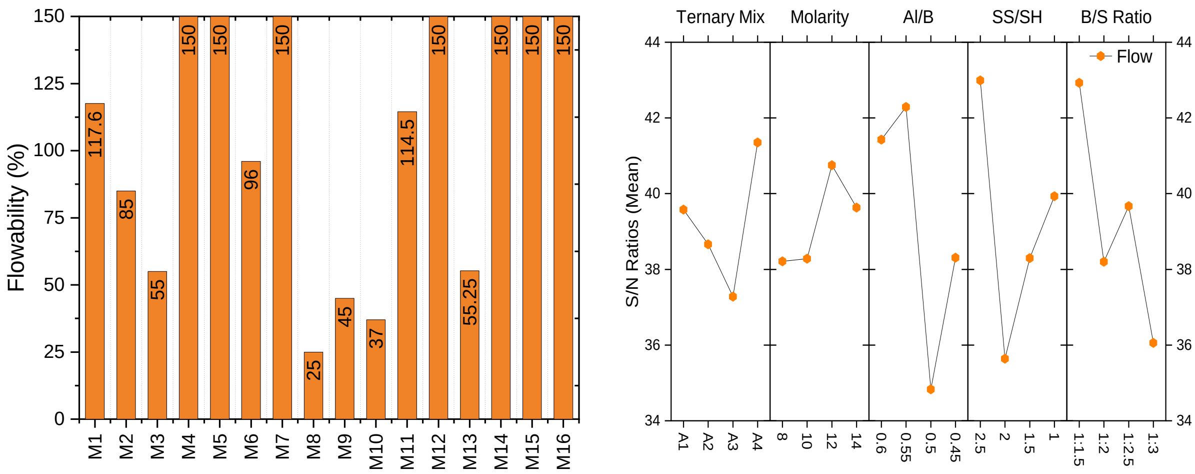


Fig. 6. Flowability of Mortars and S/N Ratios (Mean)

### 4.5 Multi Response Optimization by Taguchi Grey Relational Analysis

The optimal factor level combinations for each factor, that demonstrated superior performance for each of the response variables are identified on the basis of S/N ratios. Confirmatory experiments based on Taguchi Analysis were conducted for each individual response variable, and the results are shown in Table 8. The compressive strength of 51.94 MPa achieved after 28 days is 5.81% greater than the maximum strength determined using the L16 orthogonal array mixes. Additionally, this mix showed a shorter setting time of 25 minutes, which necessitates multi-factor optimization using the Taguchi–GRA method.

S/N ratios were normalized and transformed into Grey Relational Coefficients (GRCs) for multi-response comparison and the results are tabulated in Table 9 to identify optimal factor levels under different optimization objectives. Multi-response optimization was carried out using three different weights as shown in Table 10 to prioritize compressive strength, workability and balanced overall performance. Grey Relational Grades (GRGs) of the different optimization criteria are show in Table 11.

Table 8. Taguchi - Optimum levels of each factor for response variables

| Factors | Flowability | IST | FST | CS-07 Days | CS-28 Days |
|---|---|---|---|---|---|
| Ternary Mix | A4 | A3 | A3 | A1 | A1 |
| Molarity | 12 | 14 | 12 | 8 | 8 |
| Al/B | 0.55 | 0.5 | 0.5 | 0.45 | 0.45 |
| SS/SH | 2.5 | 2 | 2 | 1 | 1 |
| B/S Ratio | 1:1.5 | 1:1.5 | 1:1.5 | 1:1.5 | 1:1.5 |
| Confirmatory Experiment | 150 % | 96 mins | 158 mins | 46.54 MPa | 51.94 MPa |

Table 9. Grey relational coefficients based on S/N ratios for the geopolymer mortar

| | Normalized S/N Ratios | | | | | Delta | | | | | GRC | | | | |
|---|---|---|---|---|---|---|---|---|---|---|---|---|---|---|---|
| Mix No | Flow | IST | FST | CS-07 Days | CS -28 Days | Flow | IST | FST | CS -07 Days | CS -28 Days | Flow | IST | FST | CS -07 Days | CS -28 Days |
| M1 | 0.86 | 0.00 | 0.00 | 0.70 | 0.84 | 0.14 | 1.00 | 1.00 | 0.30 | 0.16 | 0.79 | 0.33 | 0.33 | 0.62 | 0.76 |
| M2 | 0.68 | 0.12 | 0.25 | 0.66 | 0.19 | 0.32 | 0.89 | 0.75 | 0.34 | 0.81 | 0.61 | 0.36 | 0.40 | 0.59 | 0.38 |
| M3 | 0.44 | 0.30 | 0.52 | 0.32 | 0.66 | 0.56 | 0.70 | 0.48 | 0.68 | 0.34 | 0.47 | 0.42 | 0.51 | 0.42 | 0.60 |
| M4 | 1.00 | 0.08 | 0.16 | 1.00 | 1.00 | 0.00 | 0.92 | 0.84 | 0.00 | 0.00 | 1.00 | 0.35 | 0.37 | 1.00 | 1.00 |
| M5 | 1.00 | 0.73 | 0.76 | 0.51 | 0.67 | 0.00 | 0.27 | 0.24 | 0.49 | 0.33 | 1.00 | 0.65 | 0.67 | 0.51 | 0.60 |
| M6 | 0.75 | 0.66 | 0.62 | 0.46 | 0.62 | 0.25 | 0.34 | 0.38 | 0.55 | 0.39 | 0.67 | 0.59 | 0.57 | 0.48 | 0.57 |
| M7 | 1.00 | 0.18 | 0.30 | 0.73 | 0.77 | 0.00 | 0.82 | 0.70 | 0.27 | 0.23 | 1.00 | 0.38 | 0.42 | 0.65 | 0.68 |
| M8 | 0.00 | 0.88 | 0.83 | 0.00 | 0.00 | 1.00 | 0.12 | 0.17 | 1.00 | 1.00 | 0.33 | 0.81 | 0.75 | 0.33 | 0.33 |
| M9 | 0.33 | 0.65 | 0.67 | 0.39 | 0.41 | 0.67 | 0.36 | 0.33 | 0.61 | 0.59 | 0.43 | 0.59 | 0.60 | 0.45 | 0.46 |
| M10 | 0.22 | 0.65 | 0.47 | 0.07 | 0.54 | 0.78 | 0.36 | 0.53 | 0.94 | 0.46 | 0.39 | 0.59 | 0.49 | 0.35 | 0.52 |
| M11 | 0.85 | 1.00 | 1.00 | 0.10 | 0.24 | 0.15 | 0.00 | 0.00 | 0.90 | 0.76 | 0.77 | 1.00 | 1.00 | 0.36 | 0.40 |
| M12 | 1.00 | 0.69 | 0.72 | 0.49 | 0.17 | 0.00 | 0.31 | 0.28 | 0.51 | 0.83 | 1.00 | 0.62 | 0.64 | 0.49 | 0.38 |
| M13 | 0.44 | 0.07 | 0.25 | 0.83 | 0.69 | 0.56 | 0.93 | 0.75 | 0.17 | 0.31 | 0.47 | 0.35 | 0.40 | 0.75 | 0.62 |
| M14 | 1.00 | 0.41 | 0.40 | 0.50 | 0.67 | 0.00 | 0.59 | 0.60 | 0.51 | 0.33 | 1.00 | 0.46 | 0.45 | 0.50 | 0.60 |
| M15 | 1.00 | 0.34 | 0.60 | 0.61 | 0.57 | 0.00 | 0.66 | 0.40 | 0.39 | 0.44 | 1.00 | 0.43 | 0.55 | 0.56 | 0.54 |
| M16 | 1.00 | 0.31 | 0.50 | 0.11 | 0.67 | 0.00 | 0.69 | 0.50 | 0.89 | 0.33 | 1.00 | 0.42 | 0.50 | 0.36 | 0.60 |

Table 10. Weighting factors for response variables under different optimization criteria's

| Optimization Criteria | Flowability | IST | FST | CS-07 Days | CS-28 Days |
|---|---|---|---|---|---|
| Balanced Overall Performance | 0.2 | 0.2 | 0.2 | 0.2 | 0.2 |
| Compressive Strength | 0.1667 | 0.1667 | 0.1666 | 0.15 | 0.35 |
| Workability | 0.5 | 0.125 | 0.125 | 0.125 | 0.125 |

Mix M4 has the highest GRG for all the three different optimizations considered. The Mix M4 has the highest reported compressive strength at the age of 7 and 28 days and flow value; nonetheless, it has quick initial and final setting times. Based on Table 12, the mean GRG analysis, distinct optimal combinations of mix parameters were identified for different optimization criteria. For balanced overall performance, the highest mean GRG was obtained at Ternary mix A2 - 60% MK, 20% GGBS, and 20%RM, 14 molar NaOH, Al/B ratio of 0.6, SS/SH ratio–1, and B/S ratio of 1:1.5, indicating a mix expected to provide balanced flowability, setting behavior, and strength development. Under the compressive strength criteria, the optimal combination corresponded to Ternary mix– A2 - 60% MK, 20% GGBS, and 20%RM, 14 molar NaOH 14, Al/B ratio–0.45, SS/SH ratio–1, and B/S ratio of 1:1.5, suggesting enhanced compressive strength performance.

Table 11. GRG's under different optimization criteria's

| Mix Designation | Balanced Overall Performance | Compressive Strength | Workability |
|---|---|---|---|
| M1 | 0.57 | 0.60 | 0.65 |
| M2 | 0.47 | 0.45 | 0.52 |
| M3 | 0.48 | 0.50 | 0.48 |
| M4 | 0.75 | 0.79 | 0.84 |
| M5 | 0.69 | 0.67 | 0.80 |
| M6 | 0.57 | 0.57 | 0.61 |
| M7 | 0.63 | 0.64 | 0.77 |
| M8 | 0.51 | 0.48 | 0.44 |
| M9 | 0.51 | 0.50 | 0.48 |
| M10 | 0.47 | 0.48 | 0.44 |
| M11 | 0.71 | 0.65 | 0.73 |
| M12 | 0.63 | 0.58 | 0.77 |
| M13 | 0.52 | 0.53 | 0.50 |
| M14 | 0.60 | 0.60 | 0.75 |
| M15 | 0.62 | 0.60 | 0.76 |
| M16 | 0.58 | 0.59 | 0.74 |

Table 12. Mean GRG response values for different optimization criteria's

| Optimization Criteria | Parameter | Level1 | Level2 | Level3 | Level4 |
|---|---|---|---|---|---|
| Balanced Overall Performance | Ternary Mix | 0.57 | 0.60* | 0.58 | 0.58 |
| | Molarity | 0.57 | 0.53 | 0.61 | 0.61* |
| | Al/B | 0.61* | 0.6 | 0.53 | 0.59 |
| | SS/SH | 0.6 | 0.55 | 0.55 | 0.61* |
| | B/S | 0.68* | 0.55 | 0.54 | 0.54 |
| Strength | Ternary Mix | 0.59 | 0.59* | 0.55 | 0.58 |
| | Molarity | 0.58 | 0.53 | 0.60 | 0.61* |
| | Al/B | 0.60 | 0.58 | 0.52 | 0.61* |
| | SS/SH | 0.61 | 0.53 | 0.56 | 0.62* |
| | B/S | 0.68* | 0.55 | 0.54 | 0.54 |
| Workability | Ternary Mix | 0.62 | 0.66 | 0.60 | 0.69* |
| | Molarity | 0.61 | 0.58 | 0.68 | 0.70* |
| | Al/B | 0.68 | 0.71* | 0.54 | 0.64 |
| | SS/SH | 0.73* | 0.55 | 0.61 | 0.67 |
| | B/S | 0.78* | 0.59 | 0.62 | 0.57 |

** Optimum Values*

For the workability criteria, the highest mean GRG was associated with Ternary mix–A4-33.33% of RM, GGBS and MK, NaOH molarity–14, Al/B ratio–0.55, SS/SH ratio–2.5, and B/S ratio of 1:1.5, indicating improved workability characteristics. The higher mean GRG implies that the mix prepared with these levels of mix parameters would perform more favorably with respect to all the evaluated properties of geopolymer concrete. Despite variations in the optimal levels of several parameters across the three criteria, 14 M NaOH molarity and B/S ratio of 1:1.5 consistently emerged as common optimal parameters on the overall performance of the geopolymer mortar irrespective of the selected optimization objective.

## 6. XRD Analysis

Among the 16 Taguchi Mixes, M4 and M8, which demonstrated the highest and lowest compressive strength respectively, were analyzed using XRD spectra as shown in Figure 7. The XRD spectra revealed crystalline phases and an amorphous component. The predominant crystalline phases derived from the raw precursor materials, including quartz ($SiO_2$), hematite ($Fe_2O_3$), and minor gibbsite or mullite, remained evident in the geopolymer mortar mixes, signifying the retention of unreacted particles from the binder materials during alkali activation. Alongside these remaining phases, new diffraction characteristics linked to geopolymerization products were detected. A wide, diffuse amorphous peak ranging from roughly 20° to 35°- 2θ was observed in all geopolymer mixtures, confirming the development of alkali-activated aluminosilicate gel phases. This indistinct area is usually attributed to the existence of C-(A)-S-H and/or N-A-S-H type gels generated during the dissolution and polycondensation of aluminosilicate species. Additionally, faint crystalline reflections associated with calcium-bearing phases, including calcite and calcium silicate hydrate-related phases, were seen, especially in mixtures with elevated GGBS content. The presence of remnant crystalline phases alongside newly generated amorphous aluminosilicate gels validates the heterogeneous characteristics of the geopolymerization process in the examined systems.

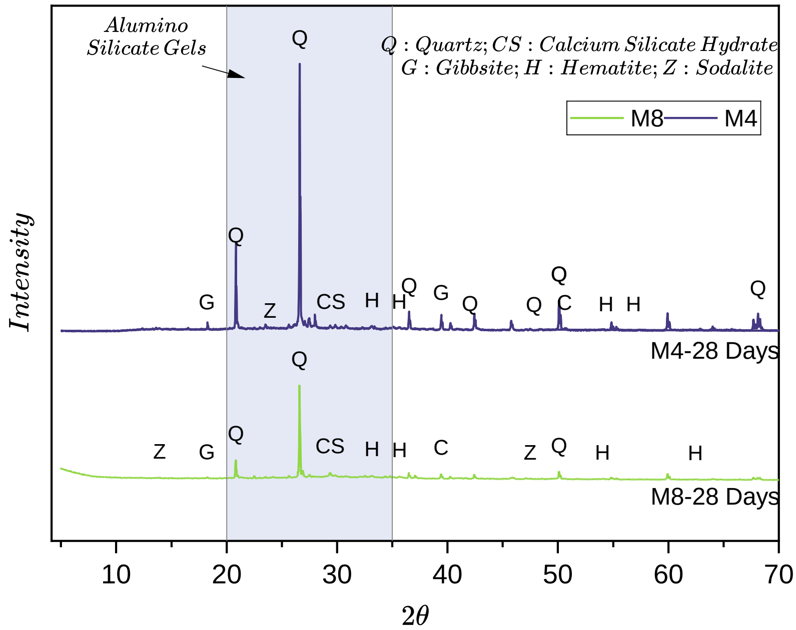


Fig. 7. XRD Spectra of GPM mixes at 28 days ambient curing

## 7. Conclusions

The integrated Taguchi and GRA methods were successfully used to develop an optimal geopolymer mortar mix that has superior performance in terms of compressive strength, flowability and setting times. This method aids in studying the effects of different factors and their corresponding levels on the desired response variables, and helps in identifying the optimal mix combinations which reduces the cost and time of experiments. The outcomes of the study are as follows:

- The ANOVA results of S/N ratios reveal SS/SH and Al/B ratio as significant factors affecting the flowability and compressive strength. The ternary mix combination of RM, GGBS and MK is the single most contributing factor for the setting times. From the Taguchi - GRA approach binder to sand ratio is the most influential factor when all the response variables are considered.
- The presence of GGBS accelerated the geopolymerization process, leading to reduced setting time and improved early-age compressive strength, while the inclusion of RM and MK played a crucial role in maintaining adequate workability and controlled setting behavior.

- The comparison of the XRD spectra of the binder materials RM, MK and GGBS with those of the ternary geopolymer mixes revealed the synthesis aluminosilicates which enhances compressive strength development. The heightened intensity of the amorphous halo in the ternary mixes with elevated GGBS concentration indicated increased gel formation, correlating with greater compressive strength at both early and later ages under ambient curing conditions.
- The Taguchi S/N ratio analysis revealed that the ternary mix containing 60% GGBS and 20% MK, 20% RM exhibited superior compressive strength performance. The Taguchi–GRA results for balanced overall performance and compressive strength identified the ternary mix comprising 60% MK and 20% GGBS, 20% RM as optimal, reflecting improved combined behavior in terms of workability, setting characteristics, and strength. This illustrates that the ideal proportions of ternary binders vary based on whether the performance objective emphasizes strength or overall balanced performance.
- The mean Grey Relational Grade (GRG) study indicated that various parameter combinations are ideal for achieving balanced performance, compressive strength, and workability. Nonetheless, a NaOH molarity of 14 M and a binder-to-sand ratio of 1:1.5 consistently proved to be ideal parameters across all optimization criteria.

The synthesized geopolymer mortar may serve as a substitute for conventional cement mortar and for precast applications. It also improves the visual appeal, attributed to its inherent red color.

## Acknowledgement

Authors acknowledge the funding received from GITAM Deemed to be University (GITAM Seed Fund: 2021/0124) and the GITAM- Nano Lab for PXRD.

## References

[1] Ghanbari M, Hadian AM, Nourbakhsh AA, MacKenzie KJD. Modeling and optimization of compressive strength and bulk density of metakaolin-based geopolymer using central composite design: A numerical and experimental study. Ceram Int 2017;43:324–35. https://doi.org/https://doi.org/10.1016/j.ceramint.2016.09.159.

[2] Pobłocki K, Pawlak M, Drzeżdżon J, Gawdzik B, Jacewicz D. Clean production of geopolymers as an opportunity for sustainable development of the construction industry. Science of The Total Environment 2024;928:172579. https://doi.org/10.1016/j.scitotenv.2024.172579.

[3] Matsimbe J, Dinka M, Olukanni D, Musonda I. Geopolymer: A Systematic Review of Methodologies. Materials 2022;15:6852. https://doi.org/10.3390/ma15196852.

[4] He J, Jie Y, Zhang J, Yu Y, Zhang G. Synthesis and characterization of red mud and rice husk ash-based geopolymer composites. Cem Concr Compos 2013;37:108–18. https://doi.org/https://doi.org/10.1016/j.cemconcomp.2012.11.010.

[5] Central Pollution Control Board ND. Guidelines for Handling and Management of Red Mud Generated from Alumina Plants 2023.

[6] Li Z, Dong H, Wang Y, Men J, Wang J, Zhao X, et al. Valorization of Alkali–Thermal Activated Red Mud for High-Performance Geopolymer: Performance Evaluation and Environmental Effects. Buildings 2025;15:2471. https://doi.org/10.3390/buildings15142471.

[7] Mounika G, Ramakrishna U, Naresh Kumar Reddy G, Suresh Kumar K. A review on effect of red mud on properties of alkali activated materials (AAMs) and geopolymers (GPs). Mater Today Proc 2023. https://doi.org/10.1016/j.matpr.2023.03.446.

[8] Anilkumar undefined, Sreekeshava KS, Bhargavi C. Studies on Optimization of Fly Ash, GGBS and Precipitated Silica in Geopolymer Concrete. Construction Materials 2025;5:29. https://doi.org/10.3390/constrmater5020029.

[9] Jin Z, Chen S, He X, Su Y, Qi H, Wang C, et al. Enhancing the mechanical properties of hemihydrate phosphogypsum-ground granulated blast-furnace slag composite binder by incorporating carbide slag as an alkaline modifier. Mater Today Commun 2025;48:113509. https://doi.org/10.1016/j.mtcomm.2025.113509.

[10] Agnihotri A, Ramana P V. GGBS: Fly-Ash evaluation and mechanical properties within high strength concrete. Mater Today Proc 2022;50:2404–10. https://doi.org/https://doi.org/10.1016/j.matpr.2021.10.257.

[11] Reddy MS, Dinakar P, Rao BH. A review of the influence of source material's oxide composition on the compressive strength of geopolymer concrete. Microporous and Mesoporous Materials 2016;234:12–23. https://doi.org/https://doi.org/10.1016/j.micromeso.2016.07.005.
[12] Nakashima H, Kurumisawa K. Reaction and microstructure of metakaolin-based geopolymer. J Sustain Cem Based Mater 2025:1–14. https://doi.org/10.1080/21650373.2025.2531266.
[13] Zheng J, Li X, Bai C, Zheng K, Wang X, Sun G, et al. Rapid fabrication of porous metakaolin-based geopolymer via microwave foaming. Appl Clay Sci 2024;249:107238. https://doi.org/10.1016/j.clay.2023.107238.
[14] H.M. T, Unnikrishnan S. Mechanical Strength and Microstructure of GGBS-SCBA based Geopolymer Concrete. Journal of Materials Research and Technology 2023;24:7816–31. https://doi.org/10.1016/j.jmrt.2023.05.051.
[15] Ma Z, Dan H-C, Tan J, Li M, Li S. Optimization Design of MK-GGBS Based Geopolymer Repairing Mortar Based on Response Surface Methodology. Materials 2023;16:1889. https://doi.org/10.3390/ma16051889.
[16] Wang L, Geddes DA, Walkley B, Provis JL, Mechtcherine V, Tsang DCW. The role of zinc in metakaolin-based geopolymers. Cem Concr Res 2020;136:106194. https://doi.org/10.1016/j.cemconres.2020.106194.
[17] Jia K, Zhou Z, Singh SV, Wang C. A review of the engineered treatment of red mud: Construction materials, metal recovery, and soilization revegetation. Results in Engineering 2024;24:102927. https://doi.org/https://doi.org/10.1016/j.rineng.2024.102927.
[18] Song W, Guo T, Han P, Wang X, Ma F, He B. Durability study and mechanism analysis of red mud-coal metakaolin geopolymer concrete under a sulfate environment. Constr Build Mater 2023;409:133990. https://doi.org/https://doi.org/10.1016/j.conbuildmat.2023.133990.
[19] Liu J, Li X, Lu Y, Bai X. Effects of Na/Al ratio on mechanical properties and microstructure of red mud-coal metakaolin geopolymer. Constr Build Mater 2020;263:120653. https://doi.org/https://doi.org/10.1016/j.conbuildmat.2020.120653.
[20] Li Z, Gao M, Lei Z, Tong L, Sun J, Wang Y, et al. Ternary cementless composite based on red mud, ultra-fine fly ash, and GGBS: Synergistic utilization and geopolymerization mechanism. Case Studies in Construction Materials 2023;19:e02410. https://doi.org/https://doi.org/10.1016/j.cscm.2023.e02410.
[21] Du Z, Sheng S, Guo J. Effect of composite activators on mechanical properties, hydration activity and microstructure of red mud-based geopolymer. Journal of Materials Research and Technology 2023;24:8077–85. https://doi.org/https://doi.org/10.1016/j.jmrt.2023.05.049.
[22] Li Z, Gao M, Lei Z, Tong L, Sun J, Wang Y, et al. Ternary cementless composite based on red mud, ultra-fine fly ash, and GGBS: Synergistic utilization and geopolymerization mechanism. Case Studies in Construction Materials 2023;19. https://doi.org/10.1016/j.cscm.2023.e02410.
[23] Prusty JK, Pradhan B. Multi-response optimization using Taguchi-Grey relational analysis for composition of fly ash-ground granulated blast furnace slag based geopolymer concrete. Constr Build Mater 2020;241:118049. https://doi.org/10.1016/j.conbuildmat.2020.118049.
[24] Hisam MW, Dar AA, Elrasheed MO, Khan MS, Gera R, Azad I. The Versatility of the Taguchi Method: Optimizing Experiments Across Diverse Disciplines. Journal of Statistical Theory and Applications 2024;23:365–89. https://doi.org/10.1007/s44199-024-00093-9.
[25] Rajesh MN, Siddaraju C, Prabhu TR, Sachit TS, Suresh R. Machine learning and Taguchi optimization technique for wear rate analysis of Al 2024/ SiC/CNT based hybrid metal matrix composites. Research on Engineering Structures and Materials 2025;11:2559–79. https://doi.org/10.17515/resm2025-810ma0308rs.
[26] Hadi MNS, Farhan NA, Sheikh MN. Design of geopolymer concrete with GGBFS at ambient curing condition using Taguchi method. Constr Build Mater 2017;140:424–31. https://doi.org/10.1016/j.conbuildmat.2017.02.131.
[27] Sadri N, Baghernejad M, Ghasemi-Fasaei R, Moosavi AA, Hardie AG. Optimizing the adsorption conditions for cadmium and lead using various synthesized adsorbents with the Taguchi method. International Journal of Environmental Science and Technology 2026;23. https://doi.org/10.1007/s13762-025-06921-4.
[28] Li Y, Huang L, Gao C, Mao Z, Qin M. Workability and mechanical properties of GGBS-RFBP-FA ternary composite geopolymer concrete with recycled aggregates containing recycled fireclay brick aggregates. Constr Build Mater 2023;392:131450. https://doi.org/https://doi.org/10.1016/j.conbuildmat.2023.131450.
[29] Jain D, Adhikary S Das, Sarker PK. Novel one-part geopolymer concrete mix design using hybrid Taguchi GRA-PCA optimization approach. Structures 2025;75:108805. https://doi.org/https://doi.org/10.1016/j.istruc.2025.108805.

[30] Kumar D, Singh S. Enhancing friction and wear performance in hybrid aluminum composites through grey relational analysis. Research on Engineering Structures and Materials 2024;10:943–56. https://doi.org/10.17515/resm2024.05ma1012tn.
[31] Bureau of Indian Standards. Coarse and Fine Aggregate for Concrete-Specification ( Third Revision). 2016.
[32] Prusty JK, Pradhan B. Multi-response optimization using Taguchi-Grey relational analysis for composition of fly ash-ground granulated blast furnace slag based geopolymer concrete. Constr Build Mater 2020;241:118049. https://doi.org/https://doi.org/10.1016/j.conbuildmat.2020.118049.
[33] Aliabdo AA, Abd Elmoaty AEM, Salem HA. Effect of water addition, plasticizer and alkaline solution constitution on fly ash based geopolymer concrete performance. Constr Build Mater 2016;121:694–703. https://doi.org/https://doi.org/10.1016/j.conbuildmat.2016.06.062.
[34] Vora PR, Dave U V. Parametric Studies on Compressive Strength of Geopolymer Concrete. Procedia Eng 2013;51:210–9. https://doi.org/https://doi.org/10.1016/j.proeng.2013.01.030.
[35] Alnkaa AA, Danish A, Yaprak H, Memiş S, Gencel O, Amran M, et al. Performance evaluation and cost analysis of ternary blended geopolymers for sustainable built environment under different curing regimes. Constr Build Mater 2023;409:133842. https://doi.org/10.1016/j.conbuildmat.2023.133842.
[36] BJ A, Parthasarathy P. Enhanced approach for geopolymer mix-design and performance evaluation: Integrating hybrid Taguchi-GRA-PCA for improved properties and behavioral insights. Constr Build Mater 2024;433:136701. https://doi.org/https://doi.org/10.1016/j.conbuildmat.2024.136701.
[37] Ferdous W, Manalo A, Aravinthan T. Bond behaviour of composite sandwich panel and epoxy polymer matrix: Taguchi design of experiments and theoretical predictions. Constr Build Mater 2017;145:76–87. https://doi.org/https://doi.org/10.1016/j.conbuildmat.2017.03.244.
[38] Ali A, uz Zaman Khan Q, Saqib Mehboob S, Tayyab A, Hayyat K, Khan D, et al. Enhancing multi-objective mix design for GGBS-based geopolymer concrete with natural mineral blends under ambient curing: A Taguchi-Grey relational optimization. Ain Shams Engineering Journal 2024;15. https://doi.org/10.1016/j.asej.2024.102708.
[39] Bureau of Indian Standards. Fresh Concrete — Methods of Sampling, Testing and Analysis Part 2: Determination of Consistency of Fresh Concrete. 2018.
[40] Bureau of Indian Standards. Methods of Sampling and Analysis of Concrete 1959.
[41] Bureau of Indian Standards. Hardened concrete – Methods of test – Part 1: Testing of strength of hardened concrete – Section 1: Compressive, flexural and split tensile strength (First Revision). 2021.
[42] Al-Majidi MH, Lampropoulos A, Cundy A, Meikle S. Development of geopolymer mortar under ambient temperature for in situ applications. Constr Build Mater 2016;120:198–211. https://doi.org/https://doi.org/10.1016/j.conbuildmat.2016.05.085.
[43] Guo S, Ma C, Long G, Xie Y. Cleaner one-part geopolymer prepared by introducing fly ash sinking spherical beads: Properties and geopolymerization mechanism. J Clean Prod 2019;219:686–97. https://doi.org/https://doi.org/10.1016/j.jclepro.2019.02.116.
[44] Al-Majidi MH, Lampropoulos A, Cundy AB. Steel fibre reinforced geopolymer concrete (SFRGC) with improved microstructure and enhanced fibre-matrix interfacial properties. Constr Build Mater 2017;139:286–307. https://doi.org/https://doi.org/10.1016/j.conbuildmat.2017.02.045.
[45] Wongpa J, Kiattikomol K, Jaturapitakkul C, Chindaprasirt P. Compressive strength, modulus of elasticity, and water permeability of inorganic polymer concrete. Mater Des 2010;31:4748–54. https://doi.org/https://doi.org/10.1016/j.matdes.2010.05.012.
[46] Nazari A, Bagheri A, Riahi S. Properties of geopolymer with seeded fly ash and rice husk bark ash. Materials Science and Engineering: A 2011;528:7395–401. https://doi.org/https://doi.org/10.1016/j.msea.2011.06.027.
[47] Riahi S, Nazari A, Zaarei D, Khalaj G, Bohlooli H, Kaykha MM. Compressive strength of ash-based geopolymers at early ages designed by Taguchi method. Mater Des 2012;37:443–9. https://doi.org/https://doi.org/10.1016/j.matdes.2012.01.030.
[48] Pavithra P, Srinivasula Reddy M, Dinakar P, Hanumantha Rao B, Satpathy BK, Mohanty AN. A mix design procedure for geopolymer concrete with fly ash. J Clean Prod 2016;133:117–25. https://doi.org/https://doi.org/10.1016/j.jclepro.2016.05.041.
[49] Dave S V, Bhogayata A. The strength oriented mix design for geopolymer concrete using Taguchi method and Indian concrete mix design code. Constr Build Mater 2020;262:120853. https://doi.org/https://doi.org/10.1016/j.conbuildmat.2020.120853.
[50] Nath P, Sarker PK. Effect of GGBFS on setting, workability and early strength properties of fly ash geopolymer concrete cured in ambient condition. Constr Build Mater 2014;66:163–71. https://doi.org/https://doi.org/10.1016/j.conbuildmat.2014.05.080.
[51] Zailani WWA, Abdullah MMAB, Zainol MRRMA, Razak RA, Tahir MFM. Compressive and bonding strength of fly ash based geopolymer mortar. AIP Conf. Proc., vol. 1887, American Institute of Physics Inc.; 2017. https://doi.org/10.1063/1.5003541.

[52] Singh S, Aswath MU, Ranganath R V. Effect of mechanical activation of red mud on the strength of geopolymer binder. Constr Build Mater 2018;177:91–101. https://doi.org/https://doi.org/10.1016/j.conbuildmat.2018.05.096.
[53] Mallikarjuna Rao G, Gunneswara Rao TD. Final Setting Time and Compressive Strength of Fly Ash and GGBS-Based Geopolymer Paste and Mortar. Arab J Sci Eng 2015;40:3067–74. https://doi.org/10.1007/s13369-015-1757-z.
[54] El-Hassan H, Ismail N. Effect of process parameters on the performance of fly ash/GGBS blended geopolymer composites. J Sustain Cem Based Mater 2018;7:122 – 140. https://doi.org/10.1080/21650373.2017.1411296.
[55] Xie J, Wang J, Rao R, Wang C, Fang C. Effects of combined usage of GGBS and fly ash on workability and mechanical properties of alkali activated geopolymer concrete with recycled aggregate. Compos B Eng 2019;164:179–90. https://doi.org/https://doi.org/10.1016/j.compositesb.2018.11.067.
[56] Lee WKW, van Deventer JSJ. The effect of ionic contaminants on the early-age properties of alkali-activated fly ash-based cements. Cem Concr Res 2002;32:577–84. https://doi.org/https://doi.org/10.1016/S0008-8846(01)00724-4.
[57] Mohapatra A, Bose P, Pandit SS, Kumar S, Alex TC. Bulk Utilization of Red Mud in Geopolymer Based Products. Advances in Sciences and Engineering 2020;12:86–91. https://doi.org/10.32732/ase.2020.12.2.86.
[58] Arjun Raj PK, Sarath D, Nagarajan P, Thomas BS. A Simplified Mix Design for GGBS–Dolomite Geopolymer Concrete Using the Taguchi Method. Iranian Journal of Science and Technology, Transactions of Civil Engineering 2024;48:3189–212. https://doi.org/10.1007/s40996-024-01354-4.
[59] Shi C, Day RL. Some factors affecting early hydration of alkali-slag cements. Cem Concr Res 1996;26:439–47. https://doi.org/https://doi.org/10.1016/S0008-8846(96)85031-9.
[60] Hou L, Li J, Lu Z. Effect of Na/Al on formation, structures and properties of metakaolin based Na-geopolymer. Constr Build Mater 2019;226:250–8. https://doi.org/https://doi.org/10.1016/j.conbuildmat.2019.07.171.
[61] Bajpai R, Shrivastava A, Singh M. Properties of fly ash geopolymer modified with red mud and silica fume: a comparative study. SN Appl Sci 2020;2. https://doi.org/10.1007/s42452-020-03665-3.
[62] Malkawi AB, Nuruddin MF, Fauzi A, Almattarneh H, Mohammed BS. Effects of Alkaline Solution on Properties of the HCFA Geopolymer Mortars. Procedia Eng 2016;148:710–7. https://doi.org/https://doi.org/10.1016/j.proeng.2016.06.581.
[63] Shilar FA, Ganachari S V, Patil VB, Nisar KS. Evaluation of structural performances of metakaolin based geopolymer concrete. Journal of Materials Research and Technology 2022;20:3208–28. https://doi.org/https://doi.org/10.1016/j.jmrt.2022.08.020.
[64] Shilar FA, Ganachari S V, Patil VB, Neelakanta Reddy I, Shim J. Preparation and validation of sustainable metakaolin based geopolymer concrete for structural application. Constr Build Mater 2023;371:130688. https://doi.org/https://doi.org/10.1016/j.conbuildmat.2023.130688.
[65] Qiu J, Zhao Y, Xing J, Sun X. Fly Ash/Blast Furnace Slag-Based Geopolymer as a Potential Binder for Mine Backfilling: Effect of Binder Type and Activator Concentration. Advances in Materials Science and Engineering 2019;2019. https://doi.org/10.1155/2019/2028109.
[66] Deb PS, Nath P, Sarker PK. The effects of ground granulated blast-furnace slag blending with fly ash and activator content on the workability and strength properties of geopolymer concrete cured at ambient temperature. Materials & Design (1980-2015) 2014;62:32–9. https://doi.org/https://doi.org/10.1016/j.matdes.2014.05.001.
[67] Aliabdo AA, Abd Elmoaty AEM, Salem HA. Effect of water addition, plasticizer and alkaline solution constitution on fly ash based geopolymer concrete performance. Constr Build Mater 2016;121:694–703. https://doi.org/https://doi.org/10.1016/j.conbuildmat.2016.06.062.
[68] Yaseri S, Hajiaghaei G, Mohammadi F, Mahdikhani M, Farokhzad R. The role of synthesis parameters on the workability, setting and strength properties of binary binder based geopolymer paste. Constr Build Mater 2017;157:534–45. https://doi.org/https://doi.org/10.1016/j.conbuildmat.2017.09.102.